

## Article

# Model Test Study on the Vertical Uplift Bearing Characteristics of Soil Continuous Solidified Pile Group Foundations

Tao Sun <sup>1</sup>, Fakai Yang <sup>1</sup>, Xinzhuang Cui <sup>2</sup>, Zhaochao Huang <sup>3</sup>, Xianzhou Lyu <sup>1,\*</sup>, Ruijin Ma <sup>4</sup>, Yujun Chang <sup>5</sup>, Shengmei Liu <sup>6</sup>, Chen Wang <sup>1</sup>, Zhiyuan Lin <sup>6</sup> and Xiaoning Zhang <sup>2</sup>

<sup>1</sup> School of Earth Science and Engineering, Shandong University of Science and Technology, Qingdao 266590, China; suntao@sdust.edu.cn (T.S.); 202183030009@sdust.edu.cn (C.W.)

<sup>2</sup> School of Civil Engineering, Chongqing University, Chongqing 400045, China; cuixz@sdu.edu.cn (X.C.); zhangxn@cqu.edu.cn (X.Z.)

<sup>3</sup> Gansu Water Resources and Hydropower Survey, Design and Research Institute Co., Ltd., Lanzhou 730030, China

<sup>4</sup> Department of Geographic Information Science, University of Redlands, Redlands, CA 92373, USA; ruijin\_ma@redlands.edu

<sup>5</sup> Ruiyuan Engineering Group Co., Ltd., Qingdao 266555, China

<sup>6</sup> Qingdao Research Institute of Surveying and Mapping, Qingdao 266033, China; 13589260331@163.com (S.L.); m15866115257@163.com (Z.L.)

\* Correspondence: lyuxianzhou0608@sdust.edu.cn

**Abstract:** To solve the problem of the high bearing capacity of structures in deep and weak soil layers, we invented a new type of pile group foundation in which the soil was continuously solidified between piles (hereinafter referred to as the SCS pile group foundation). Considering the two key factors of pile spacing and CSM depth, the antipulling load characteristics of SCS pile group foundations in dry sand were studied via indoor half-model tests and numerical simulations. The results showed that the ultimate uplift capacity of the SCS pile group foundation with a 2D–6D CSM depth was about 2–3 times that of the traditional pile group. When the stiffness of the CSM is so large that its effect can be ignored, the greater the pile spacing is, the greater the ultimate uplift capacity is. For the same pile spacing, the greater the depth of the CSM is, the greater the ultimate uplift bearing capacity is. When the CSM depth is greater than 10D, the uplift effect of the CSM can be effectively exerted, and the antipulling advantage of the SCS pile group foundation can be fully utilized. This study provided a reference for the antipulling design of SCS pile foundations.

**Keywords:** pile group foundation; continuously solidified soil between piles; ultimate uplift capacity; half-model test; numerical simulation



**Citation:** Sun, T.; Yang, F.; Cui, X.; Huang, Z.; Lyu, X.; Ma, R.; Chang, Y.; Liu, S.; Wang, C.; Lin, Z.; et al. Model Test Study on the Vertical Uplift Bearing Characteristics of Soil Continuous Solidified Pile Group Foundations. *Buildings* **2024**, *14*, 849. <https://doi.org/10.3390/buildings14030849>

Academic Editor: Eugeniusz Koda

Received: 5 February 2024

Revised: 3 March 2024

Accepted: 9 March 2024

Published: 21 March 2024



**Copyright:** © 2024 by the authors. Licensee MDPI, Basel, Switzerland. This article is an open access article distributed under the terms and conditions of the Creative Commons Attribution (CC BY) license (<https://creativecommons.org/licenses/by/4.0/>).

## 1. Introduction

As a widely used foundation in geotechnical engineering, pile foundations play a vital role in the process of transferring superstructure loads to deep soil layers. However, the bearing capacity of foundations in deep and weak soils has difficulty meeting the design requirements of high bearing capacity foundations for high-rise and super-high-rise buildings.

To solve the above problems, extensive studies have been carried out on the bearing characteristics of pile foundations. Research on the load-bearing characteristics of pile foundations in the early stage focused mainly on single-pile foundations. Al-mhaidib et al. [1] studied the pull-out characteristics of a single pile in sandy soil through large-scale model tests and found that the initial sand density and pile installation methods were the most significant factors affecting the pull-out capacity, and an installation method involving less disturbance had a higher pull-out capacity. Wang et al. [2] analyzed the distribution law of freezing force along a pile body and obtained the relationship function between freezing force, bearing capacity, and freezing temperature through an indoor pull-out model test of a

single pile in frozen soil. Maharaj et al. [3] studied the uplift bearing characteristics of piles with variable sections and noted that the bearing capacity of piles with variable sections was greater than that of straight piles with the same volume of concrete. Dong et al. [4] analyzed the influence of the burying depth of spiral piles, the burying depth of the first layer blade, and the blade spacing-to-width ratio on the uplift capacity of spiral piles through 16 field uplift tests and noted that such an influence has a critical point; beyond this point, the uplift bearing capacity of the spiral pile no longer increases obviously.

With more studies conducted on pile foundations, the research object has shifted from single piles to group piles. Yalcin et al. [5,6] studied the bearing performance of flexible piles and small group piles under eccentric and inclined loads and noted that the ultimate bearing capacity of piles depends on the eccentricity and inclination of loads, as well as the ratio of the upper layer thickness to the pile burying depth. Wang et al. [7] studied the bearing capacity of double piles under static pressure in sandy soil foundations through laboratory model tests and reported that the bearing capacity of static piles was mainly affected by the pile length and static pressure velocity, and the radial stress of piles under different pile lengths increased nonlinearly with depth and gradually converged to the passive earth pressure. Through field tests and model tests, Yang et al. and Gaaver [8,9] analyzed the influencing factors including pile burying depth, soil relative density, pile spacing, and pile group layout and found that the bearing capacity of a single pile mainly depended on the pile length–diameter ratio and soil properties, and that the pulling efficiency of small-spacing pile groups decreased with the increasing number of piles in the group. The relative density of the soil increased slightly with increasing soil mass but decreased with an increasing pile length–diameter ratio.

However, field tests may be affected by complex geological conditions, it is difficult to strictly control these variables, and indoor model tests are limited by boundary conditions and model materials. By combining these methods with numerical simulation methods, these problems can be better solved. A B E and Madhav et al. [10–12] studied the factors of pile soil viscosity, pile burying depth, group pile size, and pile spacing, and the relationship between the pile group bearing capacity, pile spacing, and pile and soil properties is obtained by numerical simulation, and they expounded upon the failure mechanism of group piles and the interactions between piles under different pile spacings. Rose [13] et al. studied the effectiveness of group piles without inner piles in clay (peripheral group piles) through numerical simulation and reported that the single-pile efficiency was greater for peripheral group piles than for complete grid group piles. Through 2D finite-element simulation, Naveen [14] found that the pile modulus, embankment modulus, and friction angle affect the arching mechanism significantly, and the arching zone can be increased by reducing these factors.

Scholars have proposed a calculation method for the uplift bearing capacity of piles based on different theories. Deshmukh [15] assumed that the axisymmetric failure surface was a cone, obtained the soil stress distribution on the axisymmetric failure surface by using the Ktter equation, and proposed an analytical solution for the ultimate uplift capacity of a pile anchor in non-viscous soil. Khatri et al. [16] proposed a formula for the ultimate uplift capacity of piles in cohesive soil where the undrained cohesion linearly increases with depth. Based on the Winkler foundation model and Timoshenko beam theory, Yang et al. [17] established a lateral vibration model of screw piles considering shear deformation and derived analytical solutions for the lateral dynamic displacement, bending moment, and shear force. Patra and Pise [18] proposed a simplified method to predict the ultimate uplift capacity of pile groups, taking into account factors such as the buried length-to-diameter ratio of the group pile and the pile spacing. Shanker [19] proposed a semiempirical analysis method to predict the uplift bearing capacity of group piles in sandy soil foundations, and the effectiveness of this method was verified by field test results. Amit et al. [20] proposed a method to predict the net ultimate bearing capacity of a single bent pile and pile group and provided a design diagram for evaluating the net ultimate bearing capacity of a pile group considering the arch effect, pile length, pile diameter, bending angle, pile surface

characteristics, pile group structure, pile spacing, soil characteristics, and other factors. Based on the Hoek–Brown failure criterion and the upper bound theorem, Liu et al. [21] derived the theoretical prediction formulas of the rock failure surface and the ultimate pull-out capacity of the pile and analyzed the influence laws of different rock mass parameters, pile parameters, and additional surface loads on the pile bearing capacity and failure range.

Moreover, scholars have proposed various techniques for soil reinforcement between piles, such as using cement slurry to reinforce the soil around the pile, improving the roughness of the pile–soil interface and thereby increasing the lateral friction resistance of the pile [22], to improve the bearing capacity of pile foundations. Ohtsuka [23] studied the influence of soil improvement in width and depth on the displacement and bending moment of highway bridge foundations and the influence of soil improvement on the nonlinear response of bridge piers and noted that the displacement of bridge piers can be effectively limited by strengthening the soil around group piles in the weak soil layer. Joo et al. [24] studied the improvement in uplift resistance of spiral piles by cement injection and found that cement injection could improve the bearing capacity and stiffness of spiral piles compared with traditional spiral piles. Zhou et al. [25] conducted a field study on the uplift capacity of prestressed high-strength concrete (PHC) piles in clay soil and the uplift capacity of such piles with strengthened surrounding soil. They found that the PHC piles and cement soils around the piles were integrated into the load transfer process. Rollins et al. [26–28] constructed cement soil retaining walls in the shallow layer of foundations around piles by high-pressure rotary spraying and carried out full-scale tests, centrifugal tests, and finite-element analyses of pile foundations under horizontal loading. The rotation stiffness and ultimate bearing capacity of the bending moment were significantly enhanced after the foundation around the pile was strengthened.

Such studies are based on the concept of soil reinforcement between piles and propose a new type of pile group foundation with the soil continuously solidified between piles (hereinafter referred to as the SCS pile group foundation) [29,30]. The continuously solidified member (CSM) is used to strengthen the soil layer between piles through foundation treatment methods such as MJS construction method, forming a continuous high-strength entity in the horizontal direction. It connects all foundation piles into a single entity at the target layer. The bearing characteristics of single piles or pile group foundations were studied via laboratory model tests, field tests, and numerical simulations. However, since the SCS pile group foundation is a completely new pile type, its uplift bearing characteristics have not been well studied. In this paper, a half-model experiment was designed to evaluate the uplift bearing characteristics of an SCS pile group foundation with or without CSM, considering the pile spacing and CSM depth. A numerical simulation was used to verify the reliability of the model experiment. On this basis, a theoretical calculation method for the ultimate uplift bearing capacity of the SCS pile group was proposed. This study can provide a reference for the antipulling design of SCS pile foundations.

## 2. Materials and Methods

### 2.1. Test Material

According to the research of Song, Sun et al. [30–33], this study used a half-model test and the sand rain method [34,35] to control the falling sand height to 120 cm (approximately 0.95 in density) to establish the model foundation.

The foundation material of the model is composed of white artificial quartz sand with good grading, and quartz sand within the range of 0.1–1 mm is selected by screening. The particle grading curve of the quartz sand is shown in Figure 1, and the basic properties are shown in Table 1.

According to Figure 1 and Table 1, the quartz sand used in the test is defined as medium sand [36] and has a good nonuniformity. The ratio of the test sand particle size to the pile diameter of the model pile is much less than 1/20; thus, the influence of the model foundation on the bearing capacity of the pile can be ignored [37,38].

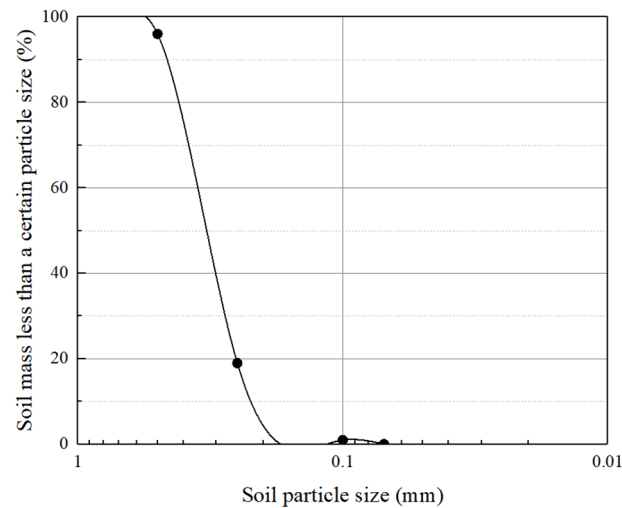


**Figure 1.** Particle grading curve.

**Table 1.** Basic physical properties of quartz sand.

| Maximum Dry Density ( $\rho_{dmax}/g \cdot cm^{-3}$ ) | Minimum Dry Density ( $\rho_{dmin}/g \cdot cm^{-3}$ ) | Specific Gravity of Soil Particle ( $G_s$ ) | Water Content ( $\omega/\%$ ) | Angle of Internal Friction ( $\phi/^\circ$ ) | $C_u$ | $C_c$ |
|---|---|---|-------------------------------|--|-------|-------|
| 1.62  | 1.31  | 2.67  | 0.042                         | 38.39  | 2.38  | 1.29  |

The materials of the model pile are made of an aluminum alloy semicircle tube, with a length of 700 mm, a diameter of 30 mm, and a wall thickness of 1.5 mm. The pile body is buried in the model foundation 600 mm deep. The ratio of the barrel diameter to the pile diameter used in the test is 26, which meets the boundary effect condition [39–41]. The CSMs are 60 mm high and 25 mm wide, and the length varies in accordance with different pile spacing. A hole with a diameter of 30 mm and a semicircular cross-section is opened on the CSM, and the model pile is tightly bonded with the CSM using a structural adhesive. The paste strain gauges were placed inside the pile body and filled with wax. Threads with a depth of 0.5 mm and a spacing of 1 mm were processed on the outer surface of the pile body to simulate the surface roughness of the pile body under actual conditions. The completed model pile is shown in Figure 2.

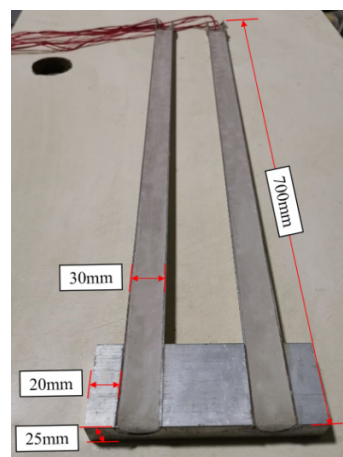


**Figure 2.** Wax injection semi-mold pile.

The test device includes a load sensor, displacement sensor, data acquisition instrument, and strain gauges [30,32,33], as shown in Figure 3.

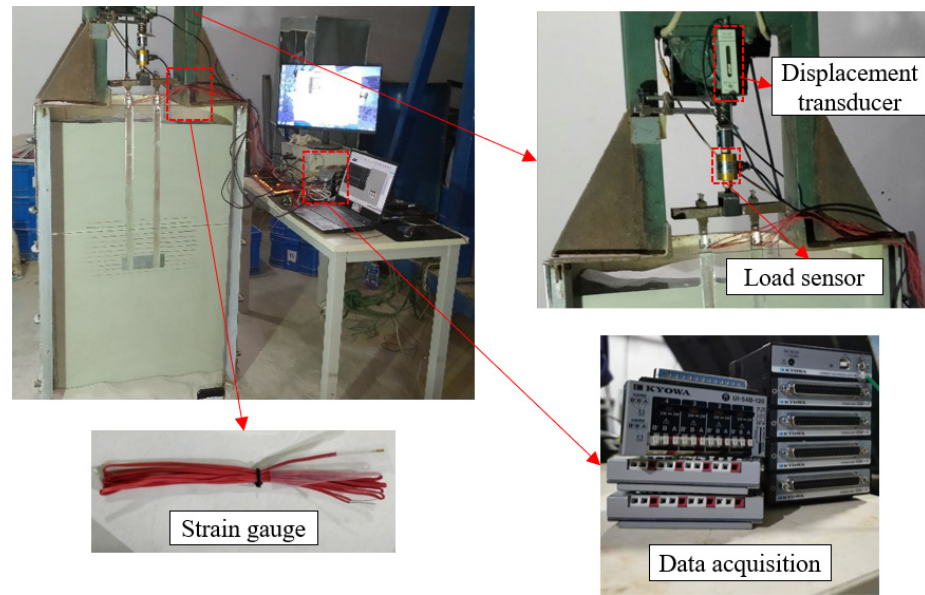


Figure 3. Test device.

2.2. Test Design

A total of 19 groups of tests were designed and carried out with a different pile spacing and CSM depth. There were 5 control test groups with different pile spacings without CSMs, 5 test groups with different pile spacings with CSMs, and 9 test groups with different CSM depths. The test model pile is shown in Figure 4.

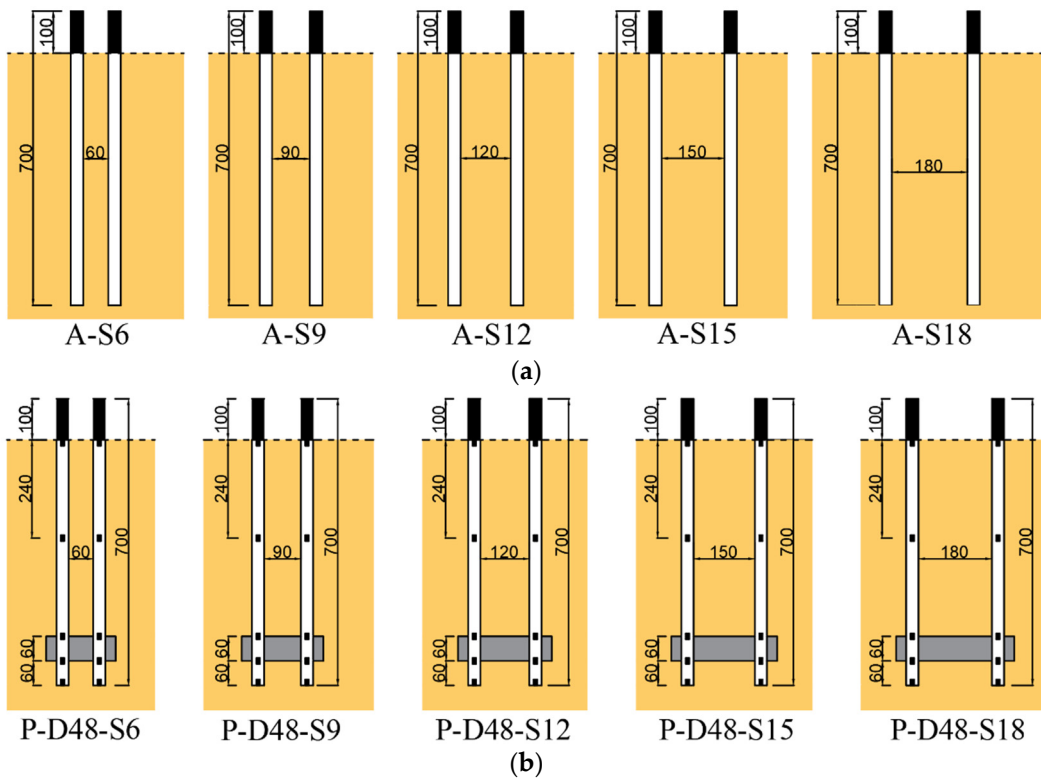
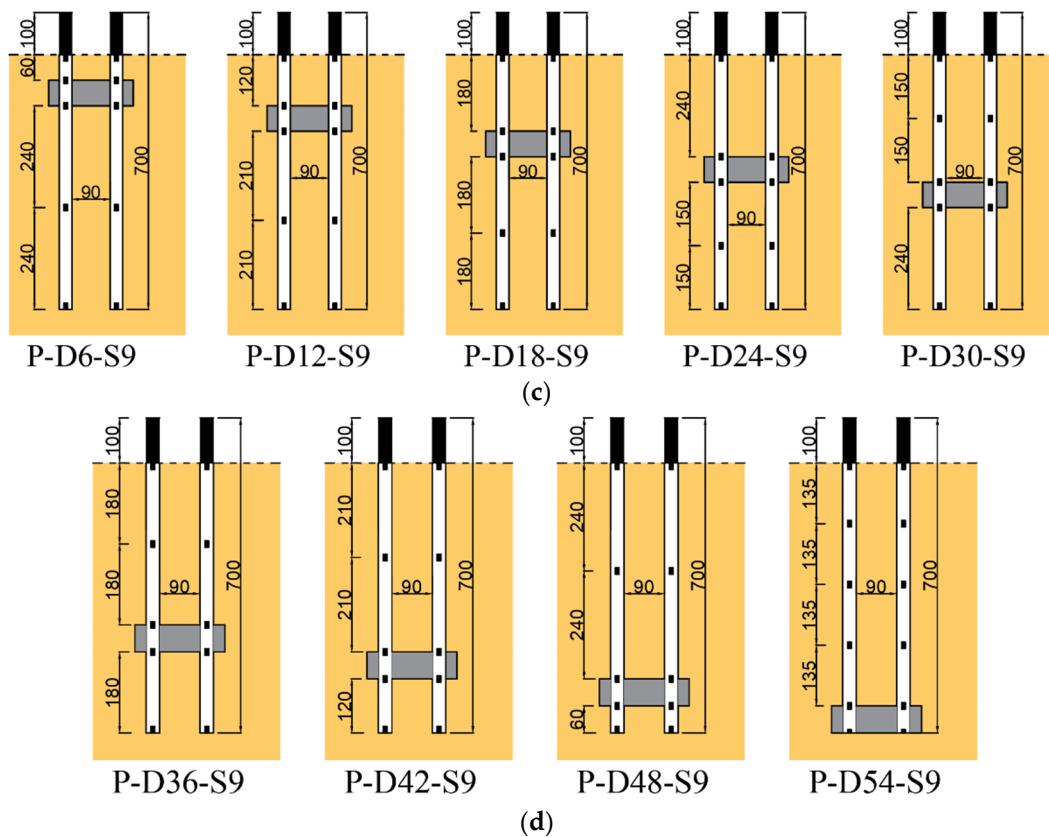


Figure 4. Cont.



**Figure 4.** Schematic diagram of test model pile (unit: mm). (a) Model piles at different pile spacing without CSM. (b) Model piles with a CSM at different pile spacing. (c) Model piles with different CSM depths-1. (d) Model piles with different CSM depths-2.

### 2.3. Test Implementation

The model foundation was constructed using the sand rain method, and the model pile was immobilized in the model bucket. The shakeout bucket filled with sand was subsequently raised to the standard height, the drop distance was 120 cm, and the density of the model foundation was controlled between 0.92 and 0.95. Each shakeout was 1 to 3 cm, the red and black dyed quartz sand was alternately deposited near the CSM with an interval of 2 cm. With the buried depth of the CSM increasing and the number of laying layers gradually increasing, the loading device and displacement acquisition device were installed after the model foundation was constructed. The test loading speed was 0.5 mm/min, and the loading was carried out through strain control. The acquisition instrument collected data every 1 s, and the test was stopped when the displacement reached 20 mm.

In the load implementation stage, the damage caused by the model pile to the foundation under vertical loading can be observed through the use of tempered glass, and the high-definition camera can shoot the whole process to clarify the failure mode of the sandy soil foundation at different load stages.

## 3. Results

### 3.1. Comparative Analysis of the Load Bearing Performance with and without a CSM

To study the uplift bearing characteristics of the SCS pile group foundation, the load–displacement curves of the A-S6 and A-S18 piles without a CSM and the P-D48-S6 and P-D48-S18 piles with a CSM were compared, as shown in Figure 5.

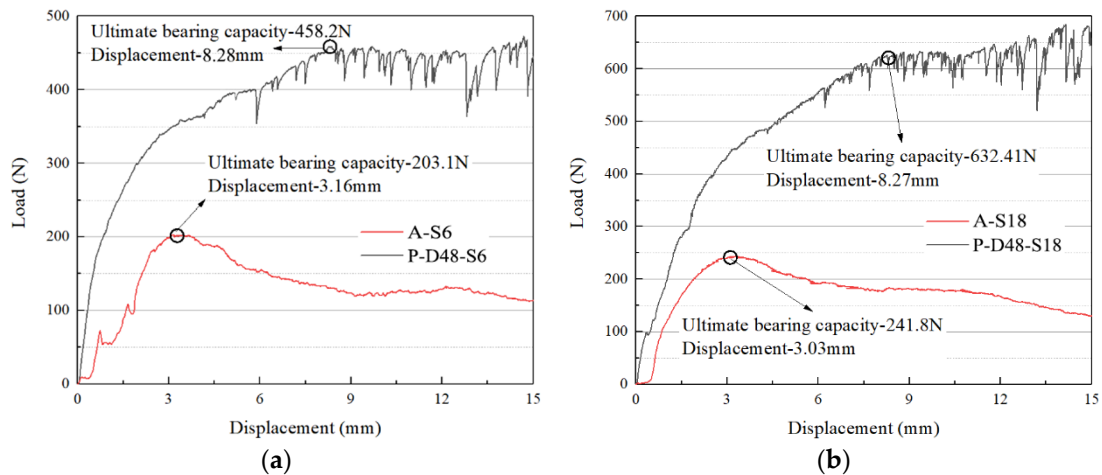


**Figure 5.** Load–displacement curve. (a) A-S6 and P-D48-S6. (b) A-S18 and P-D48-S18.

As shown in Figure 5, the curve of the SCS pile group foundation increases slowly in a wave-like manner after the load reaches its peak, while that of the traditional pile group foundation decreases after the load reaches its peak. This is mainly due to the shear of the soil under the lifting load of the pile group foundation, which results in the loss of sand particle adhesion and soil dilatancy softening. According to the load–displacement curve of the pile group foundation without a CSM, the load corresponding to the obvious inflection point of the curve is taken as the ultimate uplift capacity [42]. For the SCS pile group foundation, the load corresponding to the continuous fluctuation of the curve is taken as the ultimate uplift capacity. The ultimate uplift capacities of the Group A and P-D48 model piles are presented in Table 2.

**Table 2.** Ultimate uplift bearing capacity and displacement of group A and P-D48 model pile.

| Pile Spacing | Test Number | Ultimate Uplift Capacity (N) | Displacement (mm) | Ultimate Uplift Capacity Ratio (P-D48/A) |
|--------------|-------------|------------------------------|-------------------|--|
| 2D           | A-S6        | 203.1                        | 3.16              | 2.26                                     |
|              | P-D48-S6    | 458.2                        | 8.28              |  |
| 3D           | A-S9        | 181.2                        | 3.32              | 2.85                                     |
|              | P-D48-S9    | 516.5                        | 8.04              |  |
| 4D           | A-S12       | 215.4                        | 3.38              | 2.54                                     |
|              | P-D48-S12   | 546.6                        | 8.62              |  |
| 5D           | A-S15       | 238.0                        | 2.62              | 2.41                                     |
|              | P-D48-S15   | 574.5                        | 8.20              |  |
| 6D           | A-S18       | 241.8                        | 3.03              | 2.62                                     |
|              | P-D48-S18   | 632.4                        | 8.27              |  |

As presented in Table 2, the ultimate uplift capacity of the SCS pile group foundation with 2D–6D pile spacing is about 2–3 times that of the traditional group pile. This is mainly because the presence of an CSM increases the bearing area of the pile foundation end. The soil near the surface of the CSM is under pressure. The compressive strength of soil is known to be much greater than its shear strength. Moreover, in the process of pulling the pile foundation, the CSM can mobilize more foundation soil to participate in the load so that the soil above the CSM will be squeezed and move. Such additional normal stress generated around the pile body will continue to increase, which increases the stiffness of the soil in this part of the foundation and the side friction resistance of the pile. As a result,

the bearing capacity is increased. The test results show that the SCS pile group foundation has a significant uplift bearing advantage.

### 3.2. Influence of the Pile Spacing on the Bearing Characteristics

#### 3.2.1. Load–Displacement Curve

To study the influence of different pile spacings on the uplift bearing performance of the SCS pile group foundation, the load–displacement curves of each group under different pile spacings were drawn according to the test data, as shown in Figure 6.

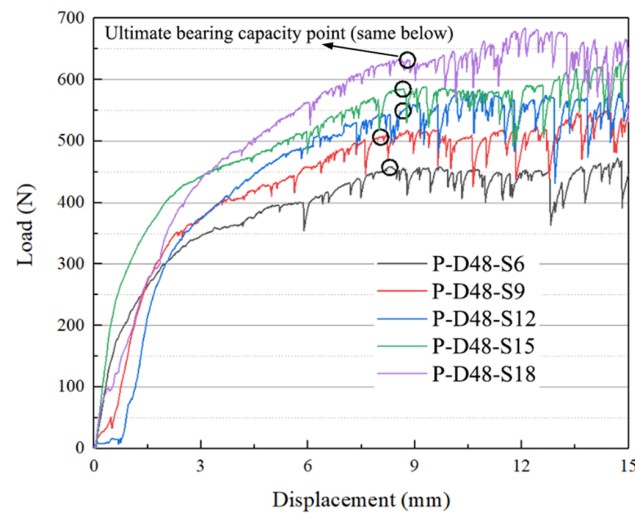


**Figure 6.** Pile load–displacement curves with different pile spacing.

In this test, the pile body was made of aluminum alloy rigid material, and the pile body and CSM were not damaged due to an excessive pulling load during the process of pulling up. As shown in Figure 6, under different pile spacings, the load–displacement curves of each group of model tests are generally the same, and the curves all exhibit a slow change, which manifests as three stages: elastic deformation, elastic–plastic deformation, and plastic failure. In the elastic stage, the lifting load of the pile increases linearly with the displacement of the pile. In the elastoplastic stage, the pile reaches the ultimate pulling capacity. After that, the curve fluctuates slowly. This is mainly due to the existence of a CSM; after the model pile reaches the ultimate uplift bearing capacity, the overall fracture surface of the foundation continues to gradually expand, so the uplift bearing capacity can still increase slowly. However, the increase in the load is too slow compared with the increase in the displacement, which is not highly important in practical engineering. The ultimate uplift bearing capacity of the model piles gradually increases with increasing pile spacing, and the SCS pile group foundations with 2D–6D pile spacing reach their ultimate bearing capacity when the displacement is approximately 8 mm. This is mainly due to the increase in the pile spacing; the bearing area of the top surface of the CSM increases so that more soil on the top of the CSM is involved in the action, and the ultimate uplift capacity of the pile group also increases.

#### 3.2.2. Axial Force Distribution of the Pile Body

The axial force of the pile body is obtained by dividing the pile body strain measured by the strain gauge attached to the inner wall of the pile body by the calibration coefficient measured by the calibration test. Since the model foundation in this test is made of dry quartz sand and the cohesion is zero, the adsorption force of the foundation on the pile bottom is not considered in the calculation of the axial force of the pile body. It is assumed that the axial force of the pile bottom is zero, and the axial force distribution diagram of the pile body of each group of model piles under different pile spacings is obtained with a CSM depth of 48 cm (16D) (Figure 7).

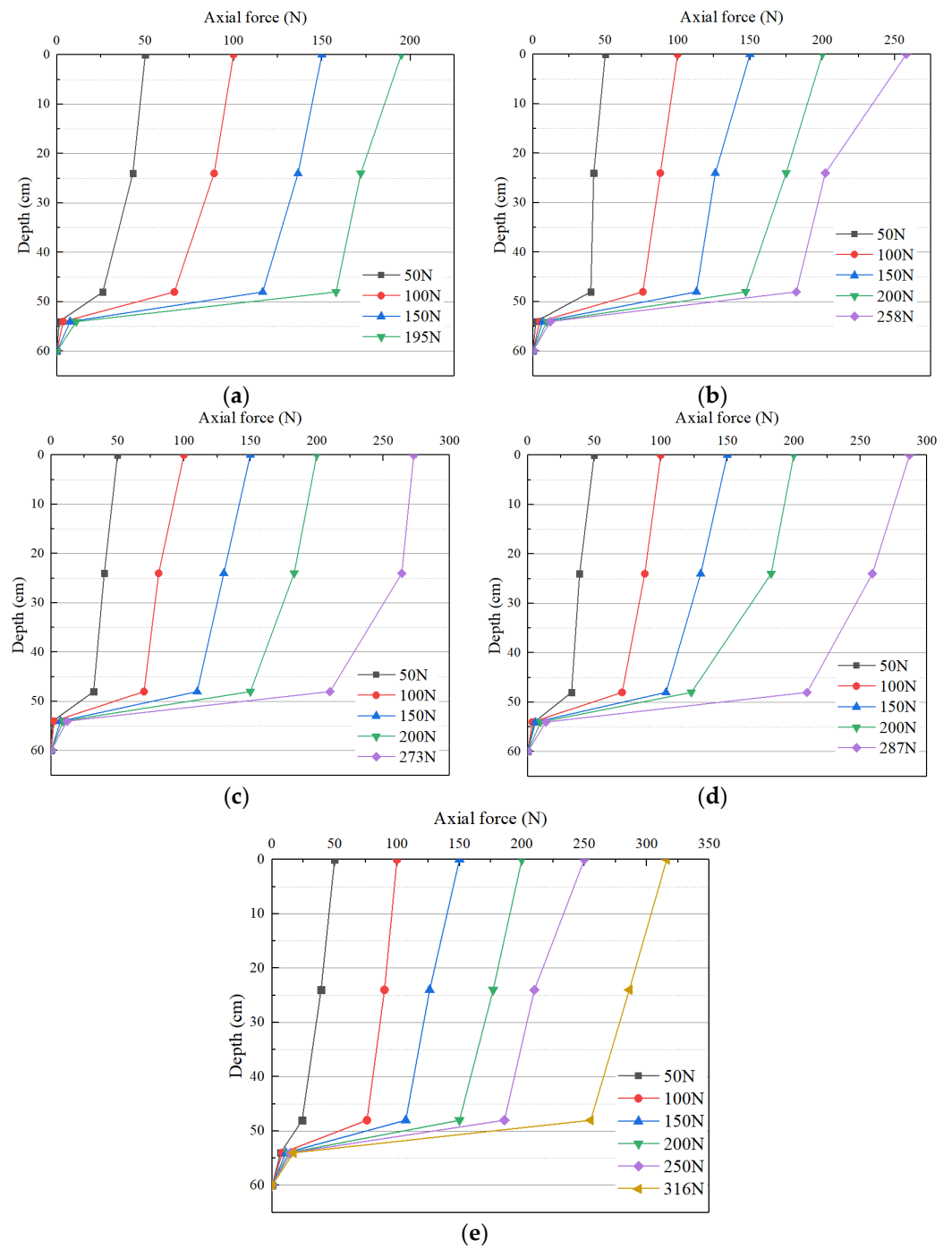


**Figure 7.** The axial force distribution curve of the P-D48 pile body. (a) P-D48-S6. (b) P-D48-S9. (c) P-D48-S12. (d) P-D48-S15. (e) P-D48-S18.

A comparison of the results in Figure 7 shows that with different pile spacings, the load transfer laws of the pile bodies of the SCS pile group foundations are similar: with increasing pile top load, the axial force of the pile body also gradually increases. Under the same load, the axial force distribution of the pile body decreases with increasing pile burying depth. The axial force of the pile decreases slowly in the upper part of the CSM and changes abruptly in the upper and lower parts of the CSM. This is mainly because, on the one hand, the setting of the CSM increases the end bearing capacity of the top surface area of the CSM; on the other hand, in the process of pile group pulling, the CSM has a

certain extrusion effect on the upper soil, which increases the stress level in the soil and subsequently increases the lateral friction resistance of the pile.

### 3.3. Influence of the CSM Depth on Bearing Characteristics

#### 3.3.1. Load–Displacement Curve

To study the influence of different CSM depths on the bearing performance of the pile, the load–displacement curves of each group of model tests under different CSM depths were drawn according to the test data, as shown in Figure 8.

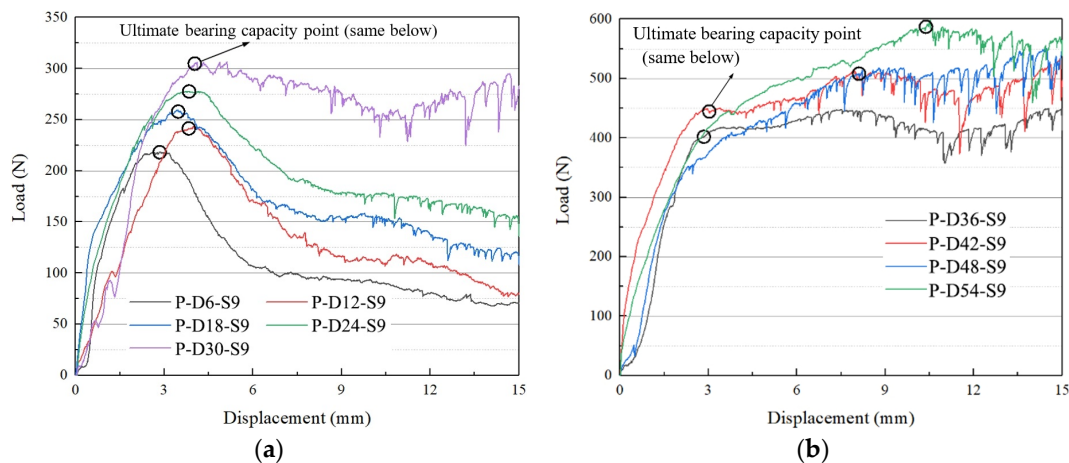


**Figure 8.** Load–displacement curves of piles with different CSM depth. (a) P-D6-S9 to P-D30-S9. (b) P-D36-S9 to P-D54-S9.

Figure 8 shows that a CSM depth leads to different load–displacement curve shapes. The load–displacement curve of the model pile with a CSM depth of  $2D\text{--}14D$  is a “steep change” type. When the P-D6-S9~P-D24-S9 model piles reach the ultimate uplift bearing capacity, the load on the top of the piles decreases rapidly. Combined with the analysis of foundation failure forms of the model mentioned above, this is mainly due to the shallow depth of CSM burying, and the stress diffusion of piles gradually reaches the surface under the uplift load, resulting in a decrease in soil strength. The results show that the pile top load decreases with increasing displacement. However, the P-D30-S9, P-D36-S9, and P-D42-S9 model piles tend to be stable after reaching the ultimate load. The load–displacement curves of the piles P-D48-S9 and P-D54-S9 are different from those of the other piles, showing a slow change and tending to stabilize after the pile top load reaches its peak. The curve of the relationship between the ultimate uplift capacity and the depth of the CSM is shown in Figure 9.

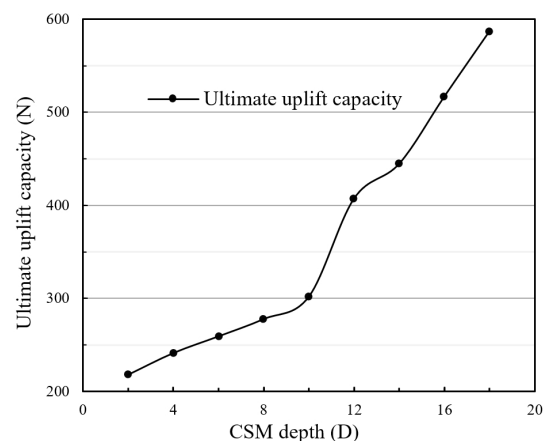


**Figure 9.** Relation curve between CSM depth and ultimate uplift capacity.

As shown in Figure 9, the ultimate uplift capacity of the piles also increases with the gradual increase in the burying depth of the CSM. When the depth of the CSM is less than 10D, the ultimate uplift capacity of the pile increases slowly with the depth of the CSM. When the burying depth is greater than 10D, the ultimate uplift capacity of the pile increases significantly with the depth of the CSM.

### 3.3.2. Axial Force of the Pile Body

The test and calculation methods in Section 3.2.2 were also adopted to obtain the axial force distribution diagram of each group of model piles under different CSM burying depths when the pile spacings were all 9 cm (3D) (Figure 10).

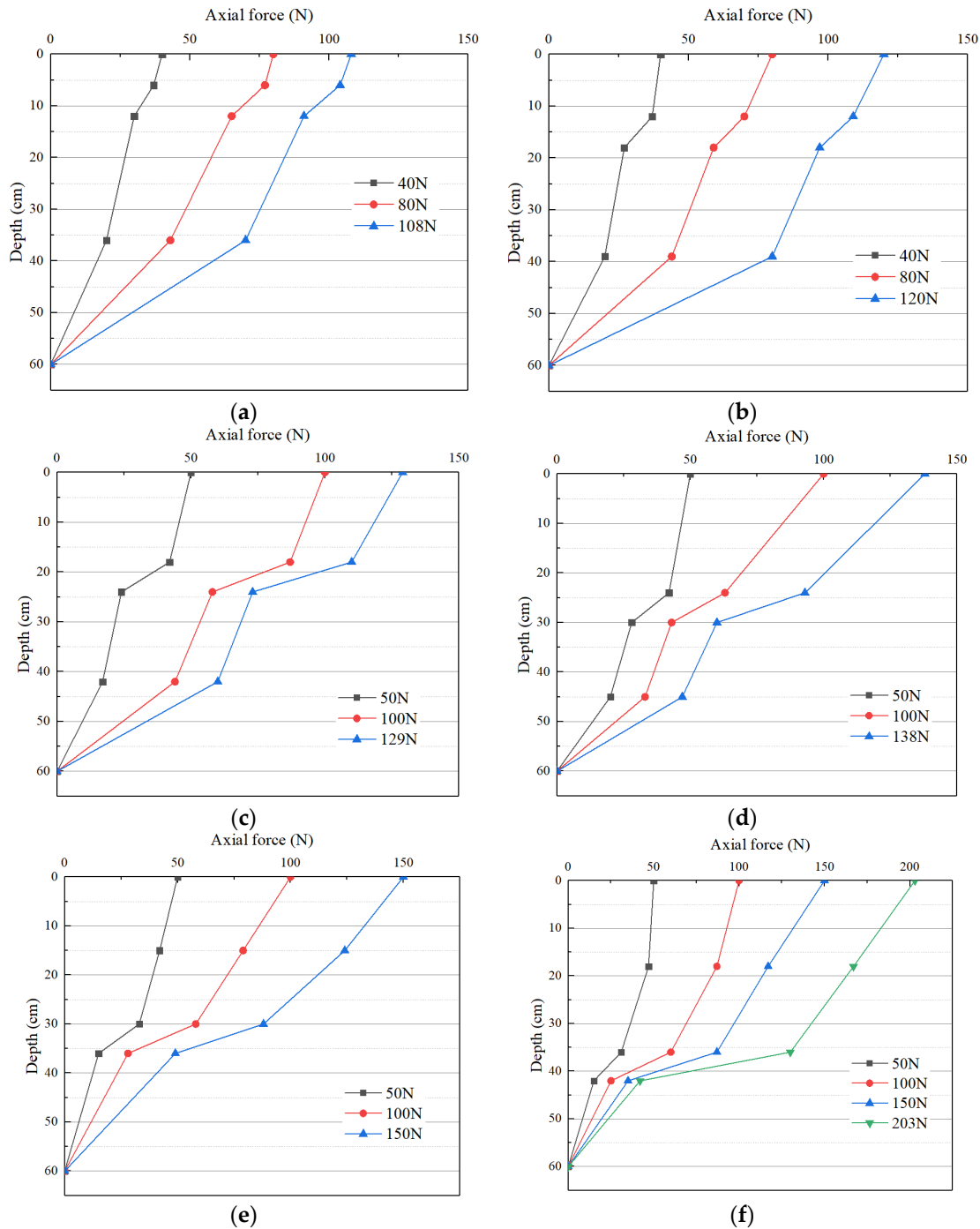
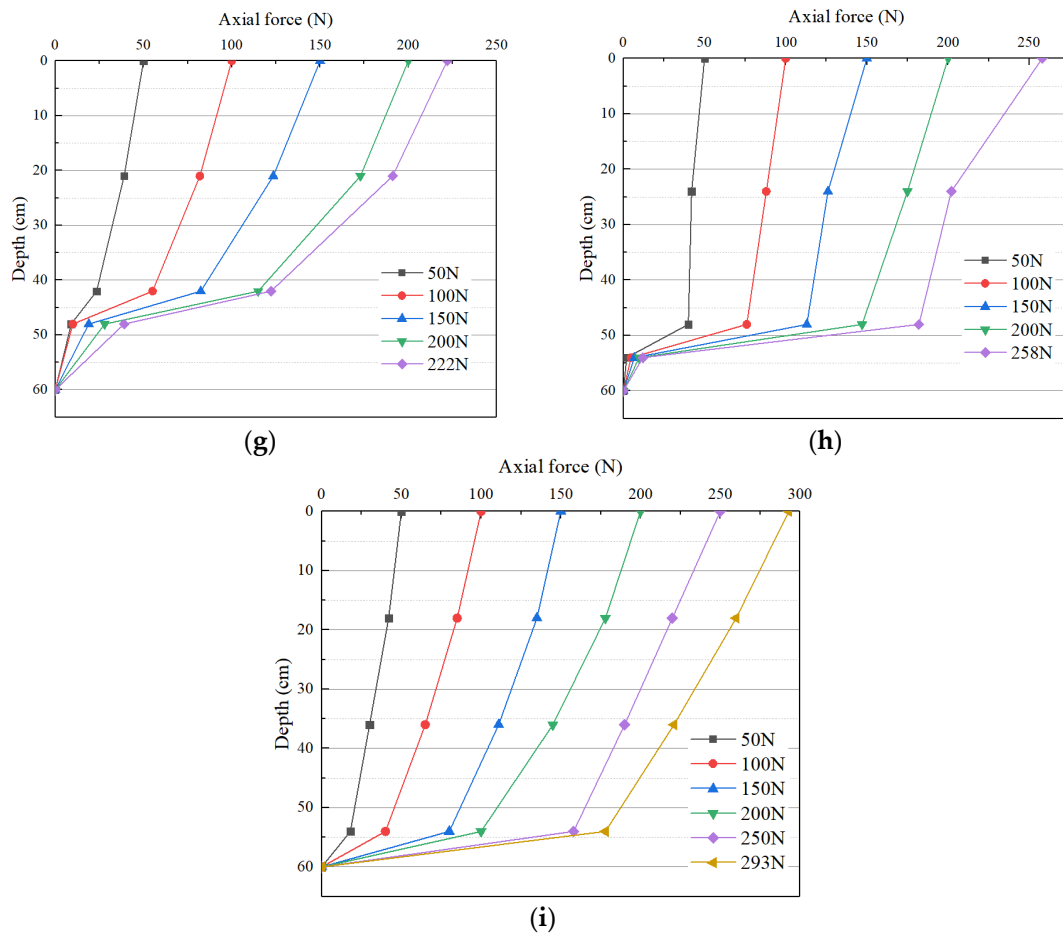


Figure 10. Cont.



**Figure 10.** Axial force distribution of the pile body. (a) P-D6-S9. (b) P-D12-S9. (c) P-D18-S9. (d) P-D24-S9. (e) P-D30-S9. (f) P-D36-S9. (g) P-D42-S9. (h) P-D48-S9. (i) P-D54-S9.

As shown in Figure 10a,b, for the model piles with 2D and 4D depths of the CSM, the axial force on the pile body above and below the CSM changes little, and the difference in axial force between the upper and lower positions of the CSM is also relatively small. This is mainly due to the shallow depth of the CSM, which is close to the surface of the model foundation, and the soil pressure on the upper part of the CSM is low. When pulling up, the CSM bears less load.

The ultimate uplift capacity of the model pile with a CSM burying depth of 6D–10D increases gradually with increasing CSM burying depth. The axial force difference between the upper and lower parts of the CSM gradually becomes obvious, as shown in Figure 10c–e.

The ultimate uplift capacity of the model pile with a CSM burying depth of 12D–18D increased with burying depth. The axial force reduction rate of the pile section with an equal section gradually slows when the CSM is used, but the axial force mutation of the pile body becomes more obvious at the upper and lower interfaces of the CSM, and the load bearing effect of the CSM gradually increases, as shown in Figure 10f–i.

By comparing the axial force distribution curves of each model pile with a CSM depth of 2D–18D, it can be found that the load transfer laws of the uplift resistant piles with different CSM depths in the pile body are similar. As the depth of CSM gradually increases, that is, the closer the pile bottom is, the greater the load borne by the CSM.

### 3.3.3. Load Sharing Ratio

Based on the axial force distribution of the pile body, the supporting force of the CSM and the lateral friction resistance of the upper and lower sections of the CSM can be calculated under each level of load. By dividing the total pile top load of each level, the

load sharing percentage of the CSM and the lateral friction resistance of the upper and lower sections of the CSM under each level of pile top load can be obtained, as shown in Figure 11.

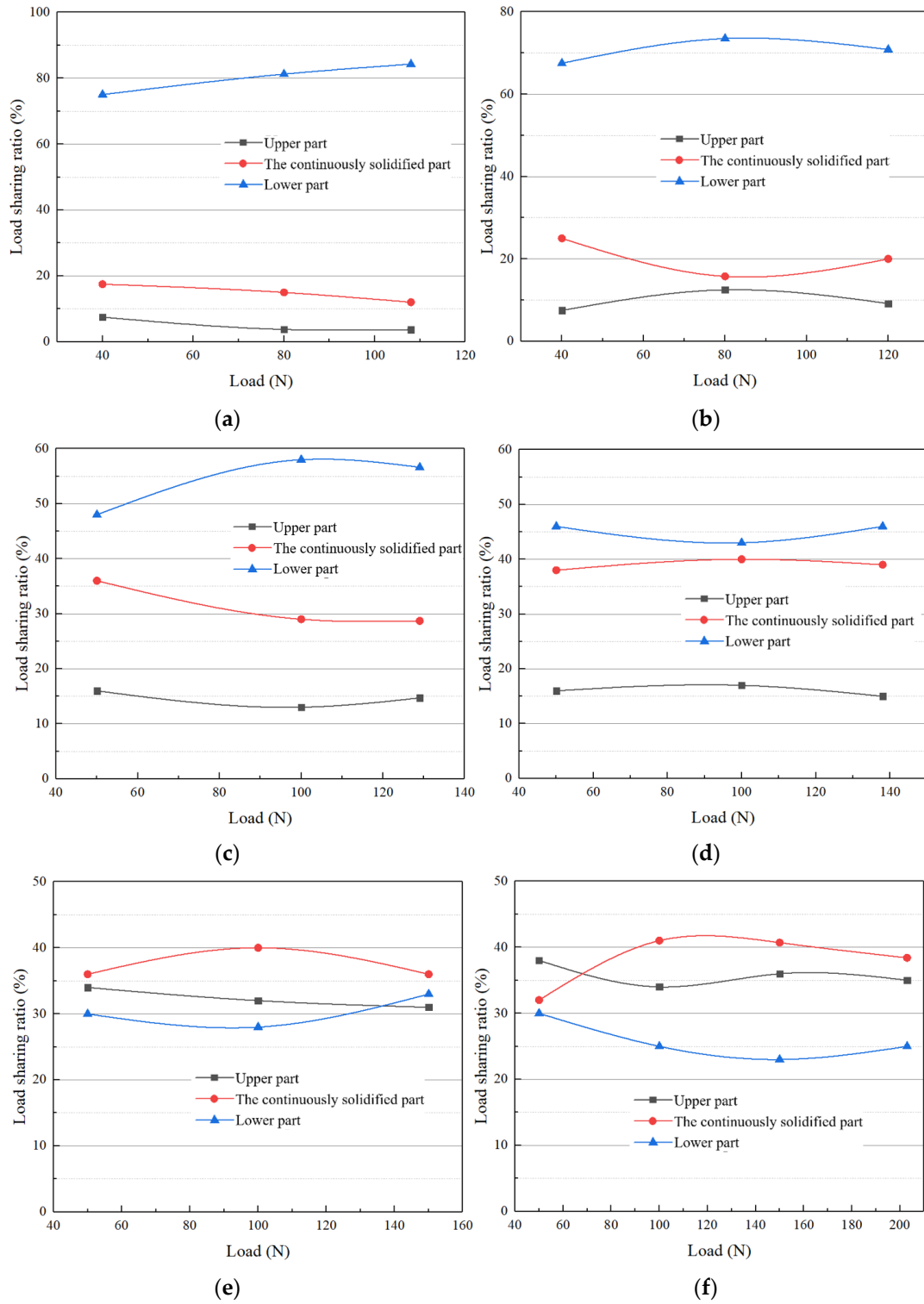
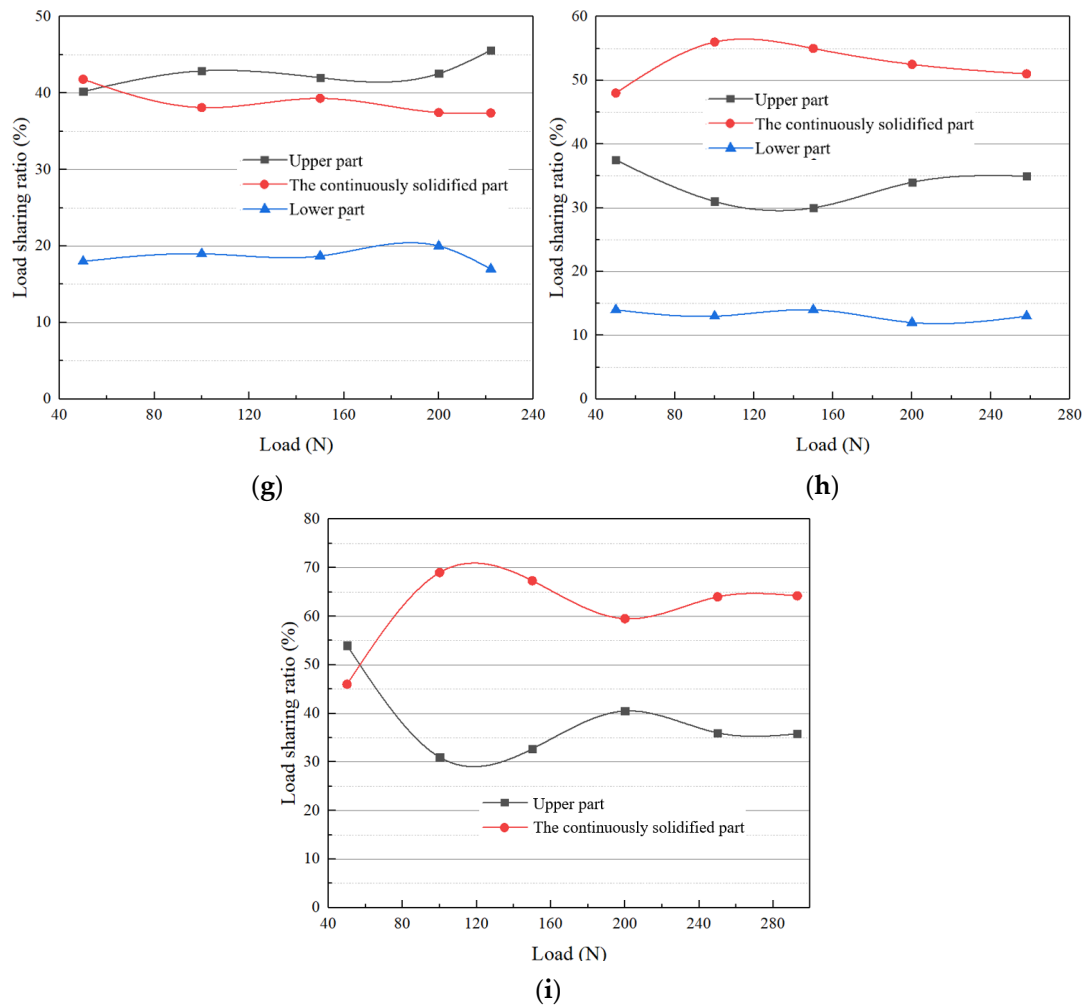


Figure 11. Cont.



**Figure 11.** Load sharing ratio of each part of the pile. (a) P-D6-S9. (b) P-D12-S9. (c) P-D18-S9. (d) P-D24-S9. (e) P-D30-S9. (f) P-D36-S9. (g) P-D42-S9. (h) P-D48-S9. (i) P-D54-S9.

The load sharing ratio of each part of the pile body indicates that the burying depth of the CSM is the main factor affecting the bearing capacity. Reasonable selection of the burying depth of a CSM can fully exploit the efficient bearing effect when the CSM is subjected to a lifting load and can avoid damage to the foundation surface through the soil. According to the test results, when the burying depth of the upper surface of the CSM is less than  $10D$ , the load is mainly borne by the side friction of the lower straight bar section. When the depth of the CSM is greater than  $10D$ , the load sharing ratio of the CSM is more than 40%, which can better support the CSM.

### 3.3.4. Damage Mode

To better study the influence of the depth of the CSM on the vertical bearing characteristics of pile group foundations, the methods of the half-model and marker layer were adopted in this experiment. Cameras were used in the experiment to shoot the whole experimental process and record the failure process of the model foundation, which helped us to explore the deformation process of the foundation more intuitively. The model foundation failure forms of each group of tests are shown in Figure 12.

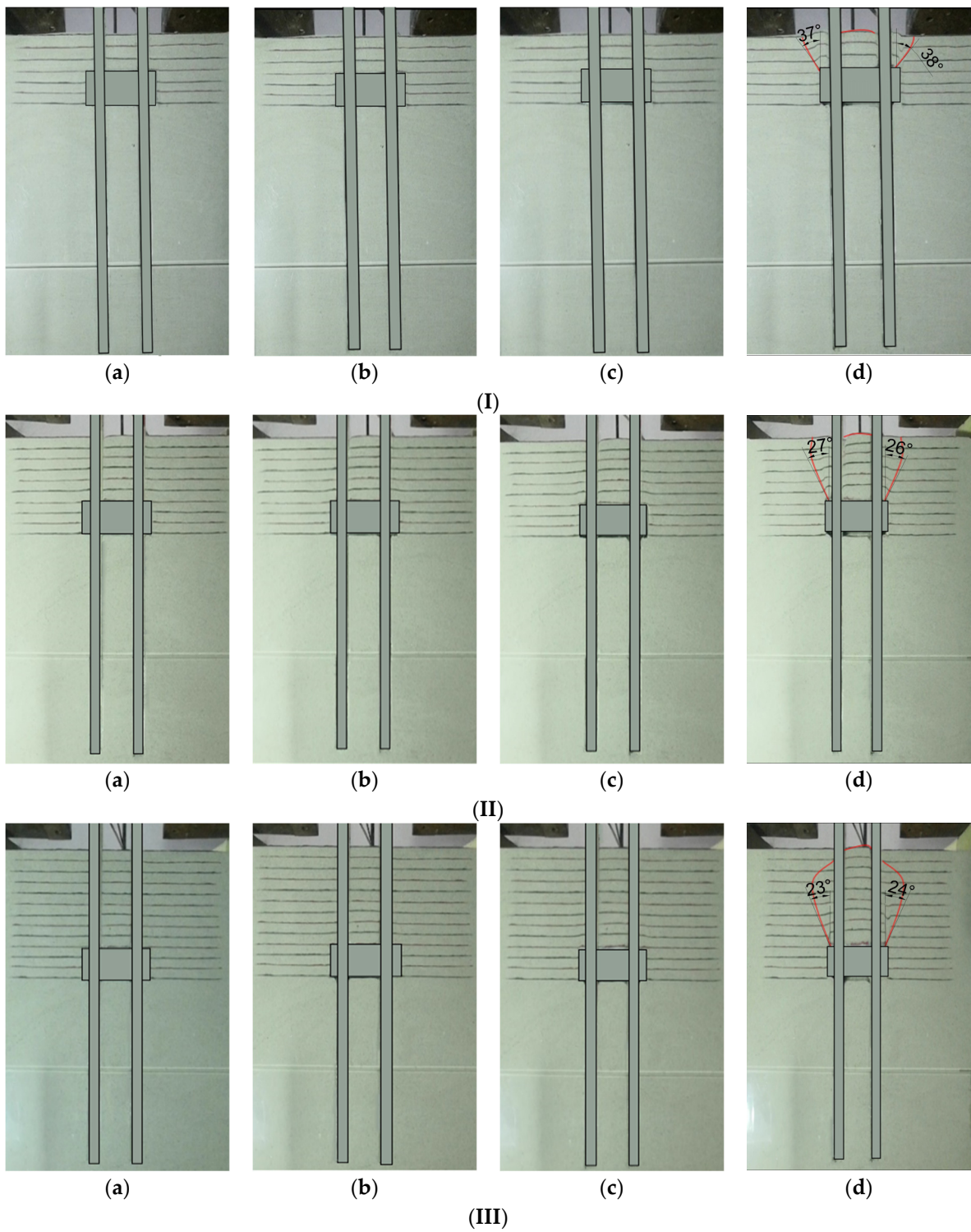


Figure 12. Cont.

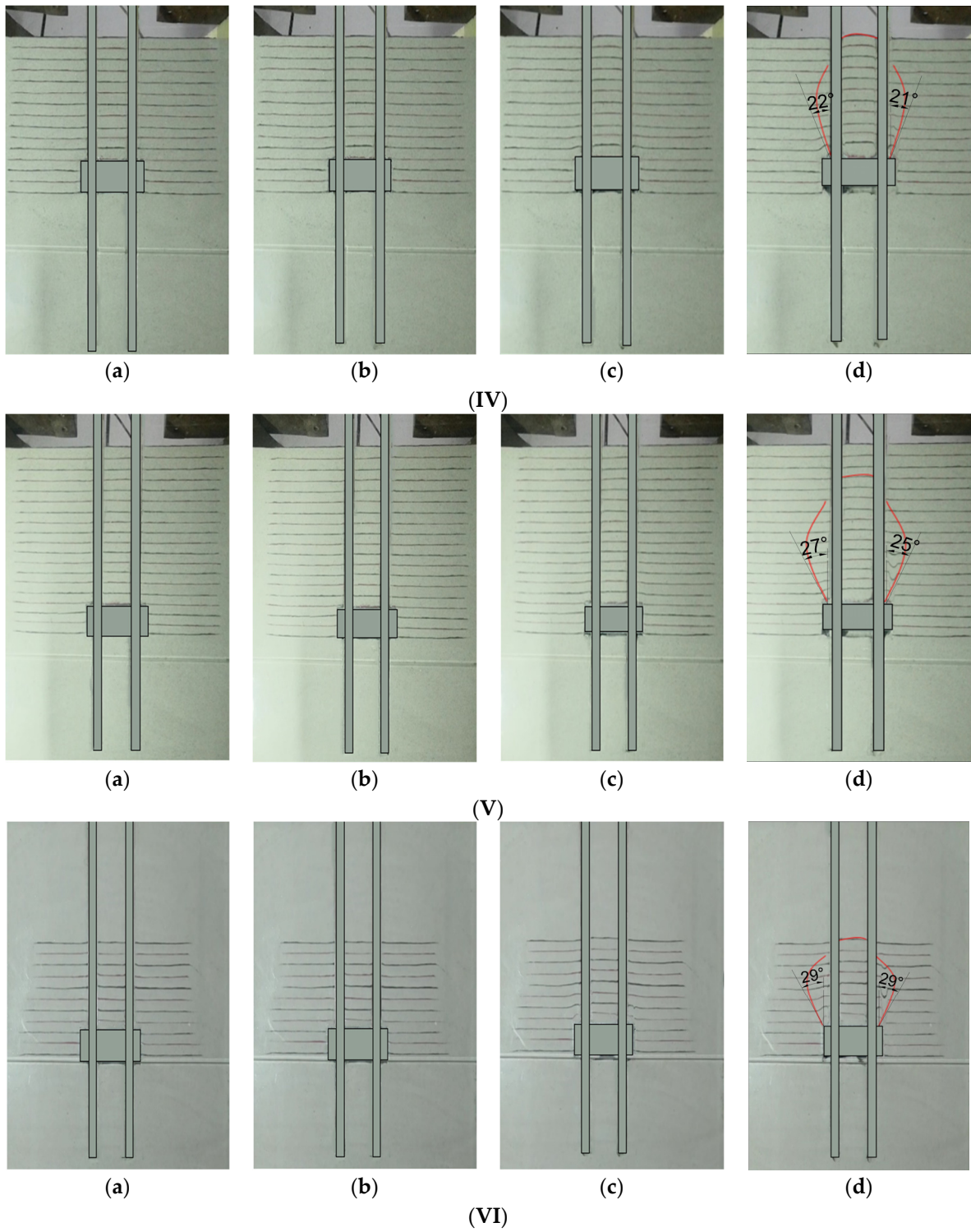
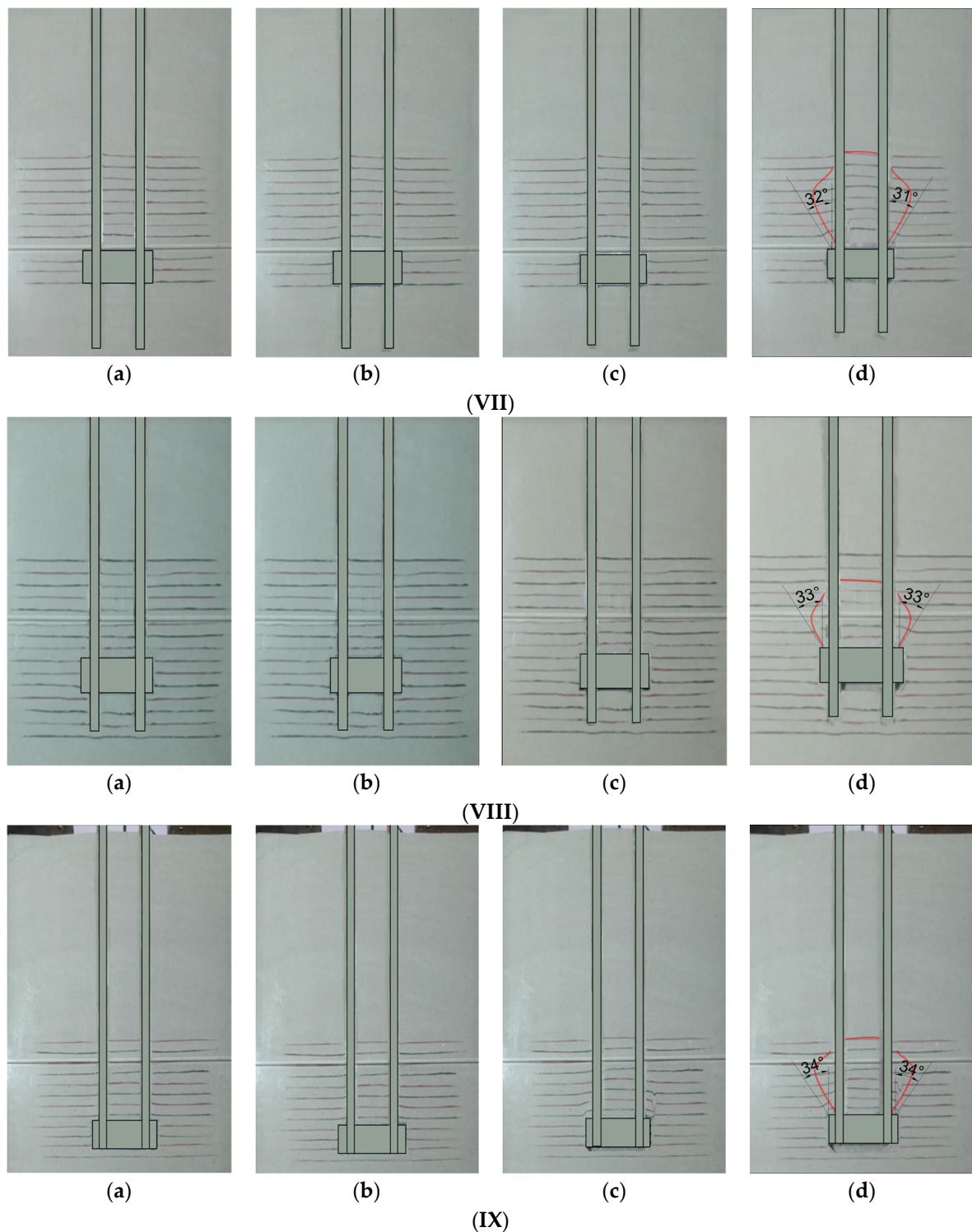


Figure 12. Cont.



**Figure 12.** Process of foundation failure. (I) P-D6-S9. (II) P-D12-S9. (III) P-D18-S9. (IV) P-D24-S9. (V) P-D30-S9. (VI) P-D36-S9. (VII) P-D42-S9. (VIII) P-D48-S9. (IX) P-D54-S9. (a) Not loaded. (b) 1/2 ultimate load. (c) Ultimate load. (d) Complete failure.

When the burying depth of the CSM is less than 12 cm (4D), before the load reaches the ultimate uplift capacity, the soil in the middle of the foundation pile and the upper part of the CSM are only in the soil compression stage, and no local shear failure of the soil mass occurs. However, the soil on both sides of the CSM will cause local shear failure in a small range. When the load exceeds the ultimate uplift capacity, overall shear failure occurs in the

middle of the two foundation piles and the upper part of the CSM of the soil, before finally penetrating the foundation surface. The shear failure surface formed by the soil on both sides of the CSM gradually approaches the foundation surface and finally penetrates it, resulting in overall failure, as shown in Figure 12(Id,IId). The depth of the CSM increases from 2D to 4D, and the angle of the fracture surface also decreases from 37 degrees to 27 degrees.

When the depth of the CSM is between 18 and 24 cm (6D–8D), after the load exceeds the ultimate uplift bearing capacity, the soil in the middle of the foundation pile and the upper part of the CSM form a fracture surface through the foundation surface. However, the shear failure surface formed by the soil on both sides of the CSM gradually diffused to the foundation surface but did not ultimately penetrate it. The vertical influence range was approximately 5D–6D, as shown in Figure 12(IIIId,IVd), and the angle of the fracture surface was maintained at approximately 22 degrees.

When the depth of the CSM is 30 cm (10D), no fracture through the foundation surface occurs during the pulling process. The soil mass in the middle of the two foundation piles and the upper part of the CSM is compressed, and the vertical influence range is approximately 8D. Local shear failure occurred on both sides of the foundation pile, which affected the soil in the range of 1D–2D in the transverse direction; the influence range in the vertical direction was approximately 7D, and the fracture plane angle was approximately 27 degrees.

When the depth of the CSM is greater than 12D, the soil above the CSM and the soil on both sides of the foundation pile are only in the soil compression stage before the load reaches the ultimate pulling capacity, as shown in Figure 12(IXb). However, when the load reaches the ultimate uplift capacity, the soil layer compression of the soil above the CSM becomes obvious, and local shear failure occurs on both sides of the foundation pile, as shown in Figure 12(IXc). Then, with increasing displacement of the pile top, the compression deformation of the soil above the CSM and the local damage range on both sides of the foundation pile also increase until the end of the test. With increasing burying depth from 12D to 18D, the fracture plane angle also increases from 29 degrees to 34 degrees.

#### 4. Numerical Simulation

To further study the vertical pull-out characteristics of the SCS pile group foundations, a numerical model of the feature group in the model test was established by using PLAXIS 3D (Version 2017, developed by Bentley Systems, 685 Stockton Drive, Exton, PA, USA) finite-element analysis software. The Mohr–Coulomb model was adopted for the sandy soil foundation. The length and width were 1200 mm, and the elastic modulus and Poisson’s ratio were set to 20 MPa and 0.25, respectively. The linear elastic model is adopted for the pile group foundation, and the elastic modulus and Poisson’s ratio are set at  $6.763 \times 10^{10}$  Pa and 0.3, respectively. Figure 13 shows the cell grid division of the pile group foundation and sandy soil foundation.

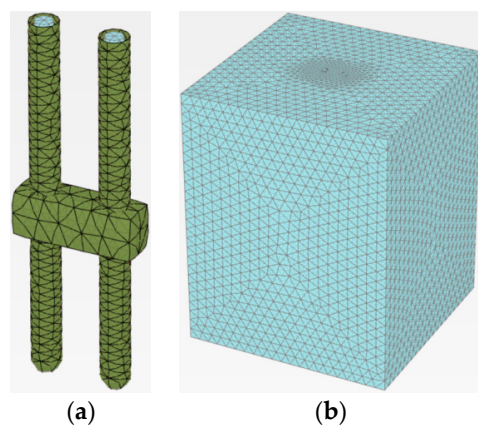


**Figure 13.** Mesh division of numerical simulation cells. (a) Grid division of pile foundation elements. (b) Grid division of sandy soil foundation elements.

To verify the reliability of the finite-element model, the numerical results of the load–displacement curves are compared with the experimental results. As shown in Figure 14, there is a good consistency between the test curve and the finite-element simulation curve. Therefore, a finite-element model can be used to qualitatively analyze the test results.

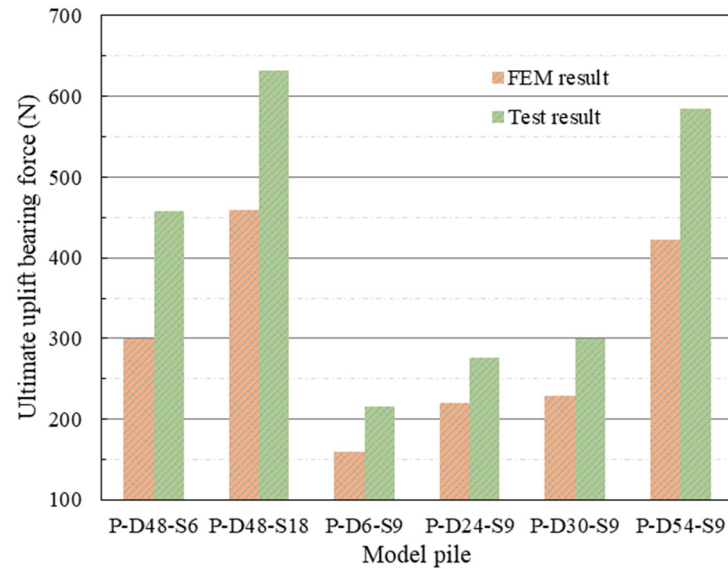


**Figure 14.** Comparison between the measured values and the simulated values.

The stress cloud map of the soil mass obtained by numerical simulation is shown in Figure 15. When the depth of CSM is 6 cm (2D), the vertical influence range runs through the surface of the foundation. When the CSM depths are 24 cm (8D) and 30 cm (10D), the vertical influence ranges are basically the same, and neither reaches the foundation surface. When the depth is CSM to 54cm (18D), the vertical influence range of the model pile on the foundation also reaches a maximum. The results obtained by numerical simulation are basically consistent with those of the model test, which verifies the accuracy of the test.

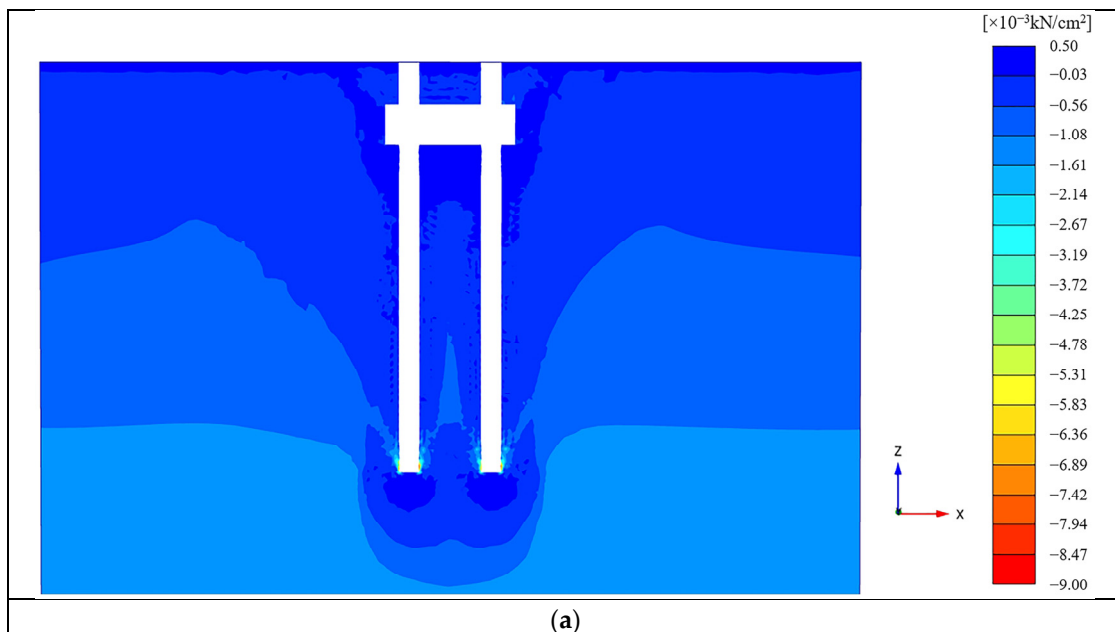


**Figure 15.** Cont.

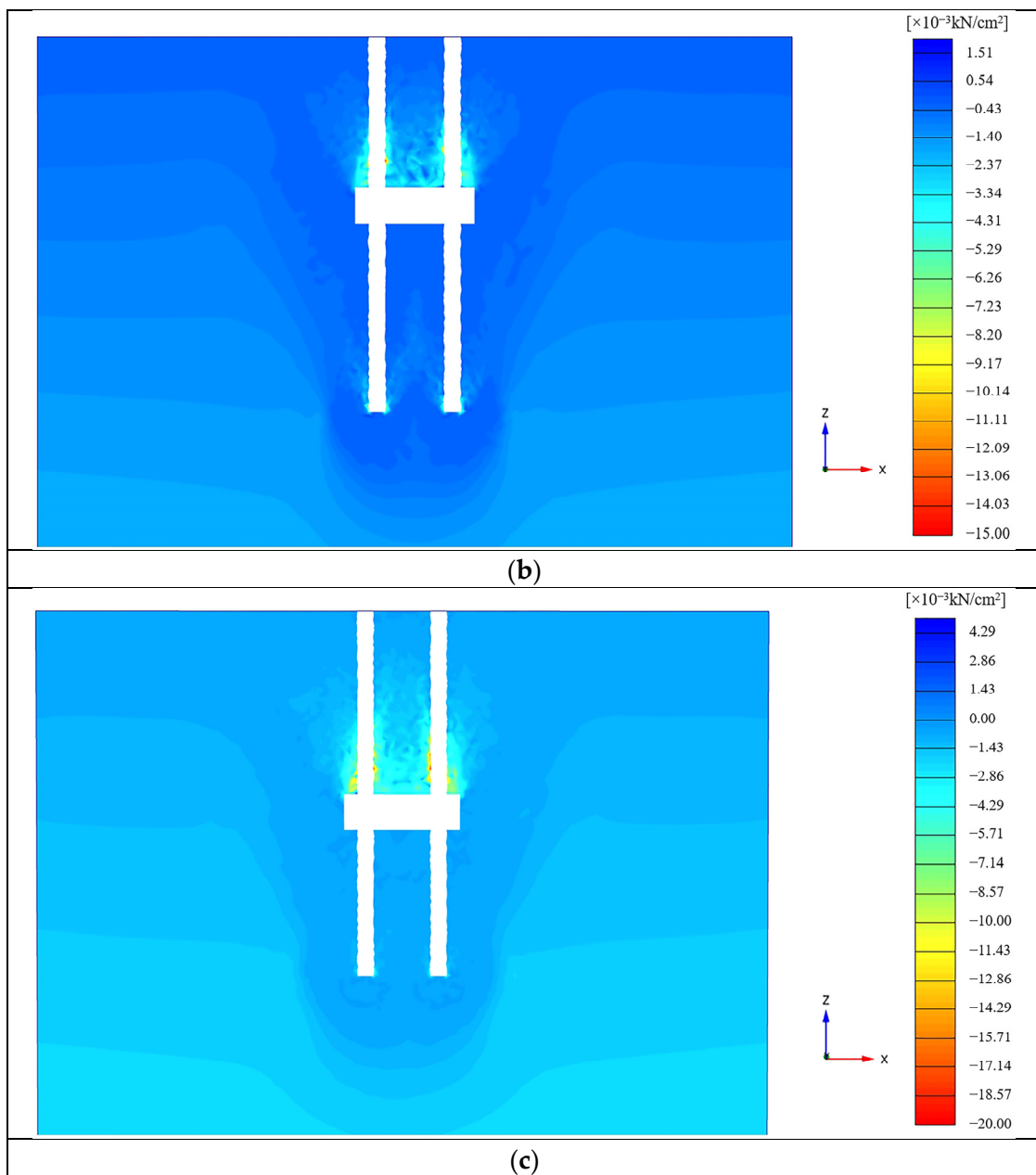


Figure 15. Cont.

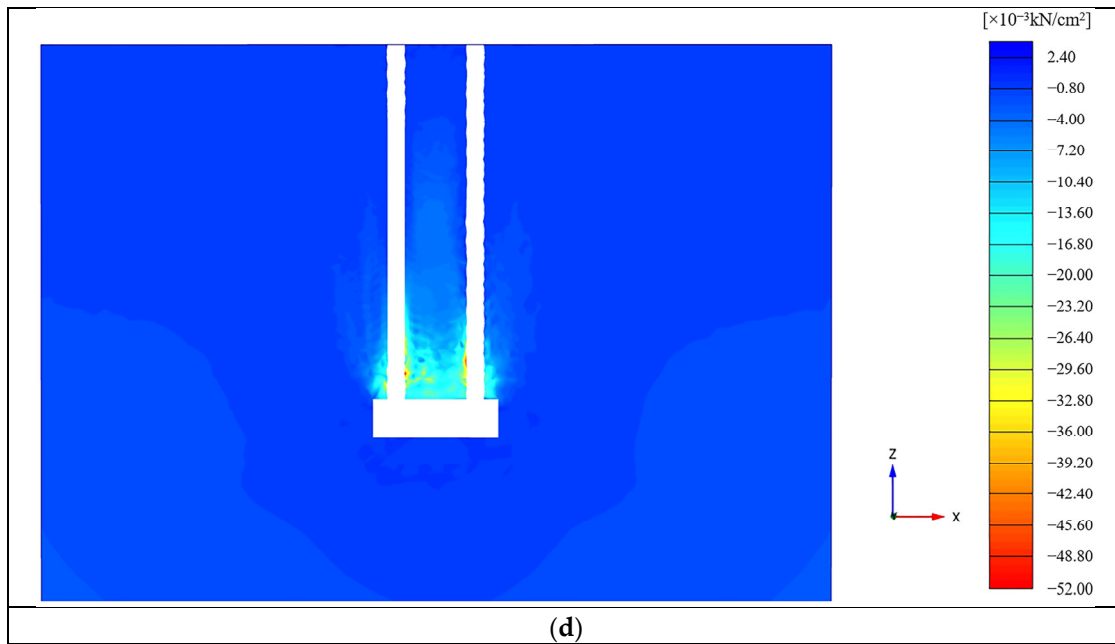


Figure 15. Stress nephogram of foundation soil. (a) P-D6-S9. (b) P-D24-S9. (c) P-D30-S9. (d) P-D54-S9.

## 5. Discussion

Referring to the research of Rui et al. [43] and considering the model in this test, the burying ratio of the SCS group pile was defined as the ratio of the burying depth of the top surface of the CSM ( $H$ ) to the length of the CSM ( $L$ ). Taking the pile spacing of 9 cm as an example ( $L = 19$  cm), the burying ratios ( $H/L$ ) at the different burying depths are 0.32, 0.63, 0.95, 1.26, 1.58, 1.89, 2.21, 2.53, and 2.84. Combined with Figures 10 and 12, it can be seen that when the burying ratio is greater than 1.58, the ultimate bearing capacity of the SCS pile group foundation increases significantly with increasing burying depth, and the load sharing ratio of the CSM exceeds 40%, which can effectively support the CSM. Accordingly, when  $H/L$  is less than 1.58, the CSM is shallow buried, and when  $H/L$  is greater than 1.58, the CSM is deep buried.

According to the research of the “Technical Code for Building Pile Foundation” (JGJ94-2008) [42] and Sun et al. [30], the theoretical formula of the ultimate uplift bearing capacity of the new pile type is derived as follows:

$$Q_u = (tu_1 + u_2) \sum \Psi_s q_{sik} l_i + \Psi_p q_{pk} A_p \quad (1)$$

where  $t$  is the number of foundation piles in the SCS pile group,  $u_1$  is the circumference of the foundation pile body,  $u_2$  is the circumference of the CSM,  $\Psi_s$  is the dimension effect coefficient of side friction resistance of the large-diameter pile, and  $q_{sik}$  is the standard value of the ultimate lateral resistance of the  $i$  layer of the pile side.  $l_i$  is the thickness of the  $i$  layer soil around the pile, and  $\Psi_p$  is the dimension effect coefficient of resistance at the tip of the large-diameter pile.  $q_{pk}$  is the standard value of the ultimate end resistance.  $A_p$  is the area of the pile end, that is, the area of the solid section.

The model pile of this test adopts a 1/20 scale model of the bored pile. The model pile with a depth of 48 cm for the CSM is selected, the specific parameters of which are enlarged according to the original scale and shown in Table 3. According to Formula (1),  $\Psi_s$  is 0.65,  $q_{sik}$  is 63 kPa,  $q_{pk}$  is 140 kPa, size effect coefficient  $\Psi_p = (0.8/d)^{\frac{1}{3}}$  ( $d$  is the diameter of the pile end), and the diameter of the pile end was the diameter of the equivalent circle of the section of the CSM. The calculation results are shown in Table 3.

Table 3. Parameters of each group of bored pile.

| Test Number | Pile Spacing (m) | Pile Number | Girth of Foundation Pile (m) | CSM Perimeter (m) | CSM Area (m <sup>2</sup> ) | Experimental Value (KN) | Calculated Value (KN) |
|-------------|------------------|-------------|------------------------------|-------------------|----------------------------|-------------------------|-----------------------|
| P-D48-S6    | 1.2              | 2           | 3.77                         | 8.4               | 5.83                       | 7331.20                 | 7539.75               |
| P-D48-S9    | 1.8              | 2           | 3.77                         | 9.6               | 7.03                       | 8264.00                 | 8214.71               |
| P-D48-S12   | 2.4              | 2           | 3.77                         | 10.8              | 8.23                       | 8745.60                 | 8834.40               |
| P-D48-S15   | 3                | 2           | 3.77                         | 12                | 9.43                       | 9192.00                 | 9451.94               |
| P-D48-S18   | 3.6              | 2           | 3.77                         | 13.2              | 10.63                      | 10,118.40               | 10,067.65             |

The relationship between calculated values and model test values can be obtained from Table 3, as shown in Figure 16.

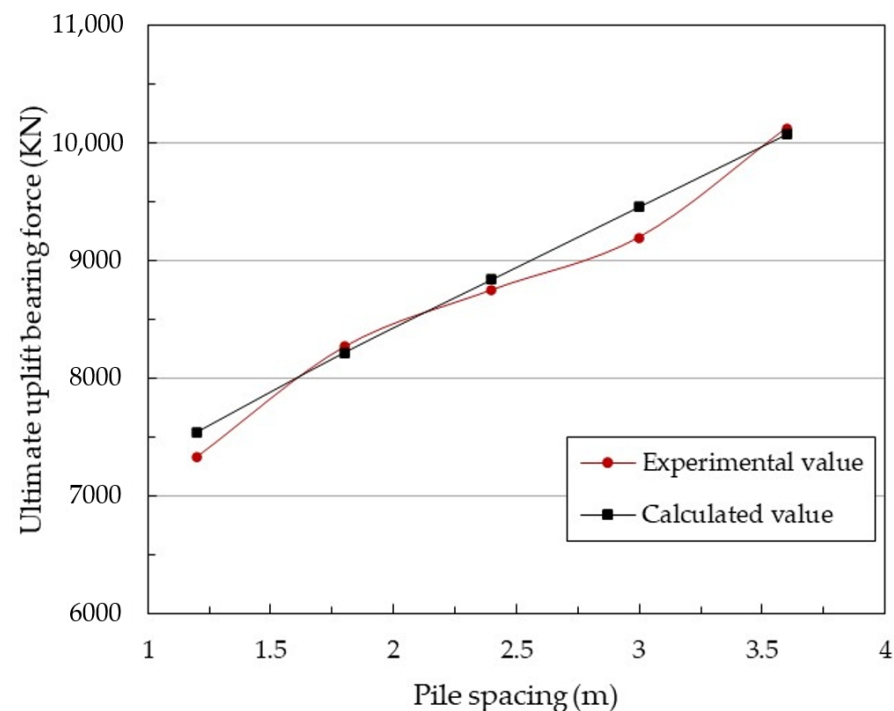


Figure 16. Comparison between calculated values and model test values.

The correlation coefficient between the test value and the calculated value can be calculated according to the Pearson correlation coefficient formula, which is defined as

$$r = \frac{\sum (x - \bar{x})(y - \bar{y})}{\sqrt{\sum (x - \bar{x})^2 \sum (y - \bar{y})^2}} \quad (2)$$

where  $r$  is the correlation coefficient,  $x$  is the calculated value,  $y$  is the experimental value,  $\bar{x}$  is the average of the calculated values, and  $\bar{y}$  is the average of the experimental values.

According to the data in Table 3, calculated by Formula (2),  $0.9 < r = 0.990 < 1$  is extremely correlated, which verifies the accuracy of the ultimate bearing capacity formula.

## 6. Conclusions

The vertical uplift bearing characteristics of a new type of SCS pile group foundation were studied. Nineteen sets of half-model tests were carried out with varying pile spacing and CSM depth as the influencing factors. The load–displacement curves and the ratios of pile axial force and load sharing obtained from the tests were analyzed; the characteristic sets in this test were simulated and analyzed via PLAXIS 3D (Version 2017, developed by

Bentley Systems, 685 Stockton Drive, Exton, PA, USA) numerical simulation software. The main conclusions are as follows:

1. When the stiffness of the CSM is large enough that its effect can be ignored and the depth of the CSM remains unchanged, the ultimate uplift capacity of the pile gradually increases with increasing pile spacing. At 2D–6D pile spacing, the SCS pile group foundation has about 2–3 times the ultimate uplift bearing capacity of the traditional pile group foundation. The loading and displacement curves of the SCS pile are relatively flat, while the axial force of the SCS group pile body changes suddenly at the upper and lower surfaces of the CSM;
2. With the same pile spacing, the ultimate uplift capacity of the pile increases gradually with CSM depth. When the burying depth of the CSM is less than or equal to 10D, the ultimate uplift capacity of the pile increases slowly with its burying depth and the top load is mainly borne by the side friction resistance of the pile. When the depth of the CSM is greater than 10D, the ultimate uplift capacity of the pile increases significantly with its burying depth and the CSM load sharing ratio exceeds 40 percent. Meanwhile, the pile top load is mainly borne by the CSM;
3. When the load exceeds the ultimate uplift capacity and the CSM depth is less than or equal to 10D, the shear failure of the soil above the SCS pile group foundation results in a penetrating fracture surface. When the CSM depth is greater than 10D, the soil compression above the CSM was apparent. Local shear failure occurred on both sides of the pile but no penetrating cracks were formed in the soil above or on the side of the CSM;
4. Numerical simulation software was used to compare and analyze the characteristic groups, and the results show that the distribution characteristics of the soil stress around the pile obtained via numerical simulation and model testing are consistent. When designing an SCS pile group foundation, the pile spacing should be as large as possible. For the same pile spacing, the depth of the CSM should be greater than 10D. The design can maximize the support of CSM, obtaining a large ultimate bearing capacity for the group pile.

**Author Contributions:** Conceptualization, T.S.; methodology, Z.L.; software, F.Y.; validation, C.W.; formal analysis, T.S. and X.L.; investigation, Z.H. and F.Y.; resources, Y.C. and S.L.; data curation, F.Y. and R.M.; writing—original draft preparation, F.Y.; writing—review and editing, X.C., X.L., R.M., Y.C., S.L., C.W. and X.Z.; visualization, X.Z.; supervision, Y.C.; project administration, Z.H. and Y.C.; funding acquisition, X.C. All authors have read and agreed to the published version of the manuscript.

**Funding:** This research was funded by the National Natural Science Foundation of China (No. 52178429, No. U22A20235 and No. 52027813) and the Natural Science Foundations of Shandong province, China (No. ZR2020ME242). And The APC was funded by T.S.

**Data Availability Statement:** The data presented in this study are available on request from the corresponding author.

**Conflicts of Interest:** Author Z.H. is employed by the company Gansu Water Resources and Hydropower Survey, Design and Research Institute Co., Ltd., Y.C. is employed by the company Ruiyuan Engineering Group Co., Ltd., S.L. and Z.L. are employed by the company Qingdao Research Institute of Surveying and Mapping. The remaining authors declare that the research was conducted in the absence of any commercial or financial relationships that could be construed as a potential conflict of interest.

## References

1. Al-Mhaidib, A.I.; Edil, T.B. Model Tests for Uplift Resistance of Piles in Sand. *Geotech. Test. J.* **1998**, *21*, 213–221. [[CrossRef](#)]
2. Wang, Z.; Wang, W.; Cheng, Y. Model Study of Tensile Bearing Capacity of a Single Pile under Frozen Condition. *J. Glaciol. Geocryol.* **2006**, *28*, 766–771.
3. Maharaj, D.K.; Gayatri, J.; Jayanthi, D. Uplift capacity of pile by finite element method. *Electron. J. Geotech. Eng.* **2004**, *9*, 4–10.
4. Dong, T.; Liang, L.; Huang, L.; Wang, M. Pullout test of screw pile foundation. *Rock Soil Mech.* **2009**, *30*, 186–190.

5. Yalcin, A.S.; Meyerhof, G.G. Bearing capacity of flexible piles under eccentric and inclined loads in layered soil: Reply. *Can. Geotech. J.* **2011**, *28*, 909–917. [[CrossRef](#)]
6. Qian, Y.; Sun, L.; Ai, L.; Zhou, Y.; Li, M. Theoretical Analysis of the Influence of Bearing Plate Position on the Bearing Performance of Soil around the CEP Antipull Force Double Pile. *Buildings* **2023**, *13*, 2613. [[CrossRef](#)]
7. Wang, Q.; Xiao, Z.; Zhao, X.; Feng, D. The Effects and Vertical Bearing Capacity of Two Jacked Model Piles in Sand. *Sustainability* **2022**, *14*, 14493. [[CrossRef](#)]
8. Yang, K.; Li, Q.; Wang, F.; Lu, C.; Wu, Y.; Ping, H. A study of failure mechanism and uplifting capacity of uplift pile foundation. *Ocean. Eng.* **1989**, *2*, 69–75.
9. Gaaver, K.E. Uplift capacity of single piles and pile groups embedded in cohesionless soil. *Alex. Eng. J.* **2013**, *52*, 365–372. [[CrossRef](#)]
10. Emirler, B.; Tolun, M.; Yildiz, A. Investigation on determining uplift capacity and failure mechanism of the pile groups in sand. *Ocean. Eng.* **2020**, *218*, 108145. [[CrossRef](#)]
11. Madhav, M.R. Efficiency of pile groups in tension. *Can. Geotech. J.* **2011**, *24*, 149–153. [[CrossRef](#)]
12. Sheil, B. Lateral limiting pressure on square pile groups in undrained soil. *Geotechnique* **2021**, *2021*, 71. [[CrossRef](#)]
13. Meena, N.K.; Nimbalkar, S.; Fatahi, B.; Yang, G. Effects of soil arching on behavior of pile-supported railway embankment: 2D FEM approach. *Comput. Geotech.* **2020**, *123*, 103601. [[CrossRef](#)]
14. Rose, A.; Taylor, R.; El Naggar, M. Numerical modelling of perimeter pile groups in clay. *Can. Geotech. J.* **2013**, *50*, 250–258. [[CrossRef](#)]
15. Deshmukh, V.; Dewaikar, D.; Choudhury, D. Uplift Capacity of Pile Anchors in Cohesionless Soil. In Proceedings of the GeoShanghai 2010: Deep Foundations and Geotechnical In Situ Testing, Shanghai, China, 3–5 June 2010. [[CrossRef](#)]
16. Khatri, V.; Kumar, J. Uplift Capacity of Axially Loaded Piles in Clays. *Int. J. Geomech.* **2011**, *11*, 23–28. [[CrossRef](#)]
17. Yang, X.; Wang, C.; Cao, S.; Wang, F.; Wu, W. Lateral Dynamic Response of Helical Pile in Viscoelastic Foundation Considering Shear Deformation. *Appl. Sci* **2023**, *13*, 12220. [[CrossRef](#)]
18. Patra, N.; Pise, P. Uplift Capacity of Pile Groups in Sand. *Electron. J. Geotech. Eng.* **2003**, *8*, 1.
19. Liu, C.; Ji, F.; Song, Y.; Wang, H.; Li, J.; Xuan, Z.; Zhao, M. Upper Bound Analysis of Ultimate Pullout Capacity for a Single Pile Using Hoek–Brown Failure Criterion. *Buildings* **2023**, *13*, 2904. [[CrossRef](#)]
20. Shanker, K.; Basudhar, P.; Patra, N. Uplift capacity of pile groups embedded in sands: Predictions and performance. *Soil Found.* **2011**, *46*, 605–612. [[CrossRef](#)]
21. Shelke, A.; Mishra, S. Uplift Capacity of Single Bent Pile and Pile Group Considering Arching Effects in Sand. *Geotech. Geol. Eng.* **2010**, *28*, 337–347. [[CrossRef](#)]
22. Li, H.; Fu, S.; Zhu, D.; Li, G.; Shen, S. Experimental study on the effects of triangular groove inclination angles on the mechanical behavior of sand–concrete interfaces. *J. Mater. Res. Technol.* **2023**, *24*, 159–172. [[CrossRef](#)]
23. Ohtsuka, T.; Aramaki, G.; Koga, K. Soil improvement of soft ground around pile foundation in earthquake-resistant design. *Low. Technol. Int.* **2004**, *6*, 42–54.
24. Santos Filho JM, D.; Tsuha CD, H. Uplift performance of helical piles with cement injection in residual soils. *Can. Geotech. J.* **2019**, *57*, 1335–1355. [[CrossRef](#)]
25. Zhou, J.; Yu, J.; Gong, X.; Zhang, R.; Yan, T. Influence of soil reinforcement on the uplift bearing capacity of a pre-stressed high-strength concrete pile embedded in clayey soil. *Soils Found.* **2019**, *59*, 2367–2375. [[CrossRef](#)]
26. Rollins, K.; Herbst, M.; Adsero, M.; Dan, B. Jet grouting and soil mixing for increased lateral pile group resistance. In Proceedings of the GeoFlorida 2010: Advances in Analysis, Modeling & Design, West Palm Beach, FL, USA, 20–24 February 2010; pp. 1563–1572.
27. Stone KJ, L.; Newson, T.A.; El Marassi, M.; El Naggar, H.; Taylor, R.N.; Goodey, R.J. An Investigation of the Use of a Bearing Plate to Enhance the Lateral Capacity of Monopile Foundations. In *Frontiers in Offshore Geotechnics II*; CRC Press: Boca Raton, FL, USA, 2010; pp. 641–646.
28. Lehane, B.; Pedram, B.; Doherty, J.; Powrie, W. Improved performance of monopiles when combined with footings for tower foundations in sand. *J. Geotech. Geoenvironmental Eng.* **2014**, *140*, 04014027. [[CrossRef](#)]
29. Sun, T. The Utility Model Relates to a Pile Group System Continuously Reinforced by Soil between Piles and a Construction Method Thereof. Chinese Patent CN106759424A, 31 May 2017.
30. Sun, T.; Wang, C.; Xu, D.; Lin, Z.; Yang, J.; Liu, S.; Yang, F. Effect of Solidified Depth on the Vertical Compressive Bearing Characteristics of the Soil Continuously Solidified Pile Group Foundation. *Appl. Sci* **2023**, *13*, 12850. [[CrossRef](#)]
31. Song, Q.; Yang, J.; Sun, T.; Li, F.; Yang, N. Model Tests on Bearing Behavior of Dynamic Deformation Process of Uplift Piles with Enlarged Base. *Period. Ocean Univ. China* **2021**, *51*, 105–112.
32. Sun, T.; Yang, J.; Zhao, H.; Sun, T.L. Study on Compressive Load-Bearing Characteristics of Section-Variable Reinforced Jet-Grouting & Mixing Cement-Soil Pile by Indoor Model Tests. *Period. Ocean Univ. China* **2012**, *42*, 8.
33. Sun, T.; Cui, X.; Sun, Y.; Han, R.; Ma, R.; Yang, J.; Wang, Y.; Chang, Y. Model tests on uplift capacity of double-belled pile influenced by distance between bells. *J. Cent. South Univ.* **2022**, *29*, 1630–1640. [[CrossRef](#)]
34. Cong, Y.; Ma, X.; Yuan, J.; Wu, P. Study on Sample Preparation with Sand Pours in Centrifuge Test. *Subgrade Eng.* **2014**, 77–80. Available online: <https://kns.cnki.net/kcms2/article/abstract?v=Vof-4b7nxdDX8dZUB2czl5N64seDVgdhQOyonOiOsvWmmcG5aBlwCeFIYp0UpXA5etaGBT3i6sUEN-k1jyanze6gduHzGUjF8gMLtzGGdnZyM9a6QMZFaNx2aa2CnFqoyImcZITpFQ=&uniplatform=NZKPT&language=CHS> (accessed on 8 March 2024).

35. Ma, X.; Kong, L.; Fang, W.; Gong, B.; Li, H.; Xu, G.; Zhao, W.; Zhang, X.; Chen, Y. Parallel tests on preparation of samples with sand pourer. *Chin. J. Geotech. Eng.* **2014**, *36*, 1791–1801.
36. GB50021-2001; Code for Investigation of Geotechnical Engineering. Ministry of Construction of the People's Republic of China: Beijing, China, 2002.
37. Garnier, J.; Konig, D. Scale effects in piles and nails loading tests in sand. *Centrifuge* **1998**, *98*, 205–210.
38. Balachowski, L. Différents Aspects de la Modélisation Physique du Comportement des Pieux: Chambre d'Ealonnage et Centrifugeuse. Ph.D. Thesis, Grenoble INPG, Grenoble, France, 1995.
39. Xu, G.; Zhang, W. Research on Particle Size Effect and Boundary Effect in Centrifugal Model. *Chin. J. Geotech. Eng.* **1996**, *18*, 80–86.
40. Mitsu, O.; Jiro, T.; Tsutomu, K. A study on bearing capacitys of shallow footings on sand. *Jpn. Soc. Civ. Eng.* **1993**, *1993*, 85–94.
41. Yang, J.; Yasuo, T. Experimental study on bearing capacity of reinforced sand. *Soil Mech. Found. Eng.* **2003**, *51*, 47–49.
42. JGJ 94-2008; Technical Code for Building Pile Foundation. Ministry of Construction of the People's Republic of China: Beijing, China, 2008.
43. Rui, R.; Xiao, F.; Cheng, Y.; Gao, F.; Hu, S.; Ding, R.; Sun, J. Experimental study on pull-out resistance of plate anchors at different buried depths. *Chin. J. Geotech. Eng.* **2023**, *45*, 2032–2041.

**Disclaimer/Publisher's Note:** The statements, opinions and data contained in all publications are solely those of the individual author(s) and contributor(s) and not of MDPI and/or the editor(s). MDPI and/or the editor(s) disclaim responsibility for any injury to people or property resulting from any ideas, methods, instructions or products referred to in the content.